Estimation of Raindrop Size Distribution Parameters from Polarimetric Radar Measurements

EUGENIO GORGUCCI

Istituto di Fisica dell'Atmosfera, Consiglio Nazionale dell Ricerche, Rome, Italy

V. CHANDRASEKAR AND V. N. BRINGI

Colorado State University, Fort Collins, Colorado

GIANFRANCO SCARCHILLI

Istituto di Fisica dell'Atmosfera, Consiglio Nazionale dell Ricerche, Rome, Italy

(Manuscript received 25 May 2001, in final form 14 February 2002)

ABSTRACT

Estimation of raindrop size distribution over large spatial and temporal scales has been a long-standing goal of polarimetric radar. Algorithms to estimate the parameters of a gamma raindrop size distribution model from polarimetric radar observations of reflectivity, differential reflectivity, and specific differential phase are developed. Differential reflectivity is the most closely related measurement to a parameter of the drop size distribution, namely, the drop median diameter (D_0). The estimator for D_0 as well as other parameters are evaluated in the presence of radar measurement errors. It is shown that the drop median diameter can be estimated to an accuracy of 10%, whereas the equivalent intercept parameter can be estimated to an accuracy of 6% in the logarithmic scale. The estimators for the raindrop size distribution parameters are also evaluated using disdrometer data based simulations. The disdrometer based evaluations confirm the accuracy of the algorithms developed herein.

1. Introduction

Ever since the introduction of differential reflectivity (Z_{dr}) measurement, one of the long standing goals of polarimetric radar has been the estimation of the raindrop size distribution (DSD). Seliga and Bringi (1976) showed that Z_{dr}, for an exponential DSD, is directly related to the median volume diameter (D_0). Careful intercomparisons between radar measurements of Z_{dr} and D_0 derived from surface disdrometers and airborne imaging probes have shown that D_0 can be estimated to an accuracy of about 10%–15% (see, for example, Aydin et al. 1987; Bringi et al. 1998). A general gamma distribution model was suggested by Ulbrich (1983) to characterize the natural variation of the DSD. The nonspherical shape of raindrops results in anisotropic propagation of electromagnetic waves, with a difference in the propagation constant at horizontal and vertical polarization states. The specific differential propagation phase (K_{dp}) is a forward scatter measurement (Seliga and Bringi 1978; Sachidananda and Zrnić 1987) whereas the radar reflectivity (Z_h) and Z_{dr} are backscatter measurements. The weighting of the DSD by Z_{dr} and K_{dp} is controlled by the variation of mean raindrop shape with size. A combination of the three radar measurements (Z_h, Z_{dr}, and K_{dp}) can be utilized to estimate the DSD, specifically the parameters of a parametric form of the DSD such as the gamma DSD. This paper presents algorithms for the estimation of parameters of a gamma DSD from polarimetric radar measurements. The paper is organized as follows. Section 2 describes the raindrop size distribution and its parameters, whereas section 3 describes the shape of raindrops and its implication for polarimetric radar measurements. Estimators of the DSD parameters are presented in section 4, and the impact of measurement errors on the estimates are discussed in section 5. Validation of the algorithms using disdrometer data are presented in section 6. Important results of this paper are summarized in section 7.

2. Raindrop size distribution

The raindrop size distribution describes the probability density distribution function of raindrop sizes. In practice, the normalized histogram of raindrop sizes (normalized with respect to the total number of observed

Corresponding author address: Dr. Eugenio Gorgucci, Istituto di Fisica dell'Atmosfera, CNR, Area di Ricerca Roma-Tor Vergata, Via del Fosso del Cavaliere, Rome 100-00133, Italy.
E-mail: gorgucci@radar.ifa.rm.cnr.it

raindrops) converges to the probability density function of raindrop sizes. A gamma distribution model can adequately describe many of the natural variations in the shape of the raindrop size distribution (Ulbrich 1983). The gamma raindrop size distribution can be expressed as,

$$N(D) = n_c f_D(D) \ (\mathrm{m^{-3}\ mm^{-1}}), \tag{1}$$

where $N(D)$ is the number of raindrops per unit volume per unit size interval (D to $D + \Delta D$), n_c is the number concentration, and $f_D(D)$ is the probability density function (pdf). When $f_D(D)$ is of the gamma form it is given by

$$f_D(D) = \frac{\Lambda^{\mu+1}}{\Gamma(\mu + 1)} e^{-\Lambda D} D^{\mu}, \qquad \mu > -1, \tag{2}$$

where Λ and μ are the parameters of the gamma pdf. Any other gamma form such as the one introduced by Ulbrich (1983),

$$N(D) = N_0 D^{\mu} e^{-\Lambda D}, \tag{3}$$

can be derived from this fundamental notion of raindrop size distribution. It must be noted that any function used to describe $N(D)$ when integrated over D must yield the total number concentration, to qualify as a DSD function. This property is a direct consequence of the fundamental result that any probability density function must integrate to unity. When $\mu = 0$, the gamma DSD reduces to the exponential form as $N(D) = n_c \Lambda e^{-\Lambda D}$. The relation between D_0, μ, and Λ is given by (Ulbrich 1983)

$$\Lambda D_0 \cong 3.67 + \mu, \tag{4}$$

where D_0 is the drop median diameter defined as

$$\int_0^{D_0} D^3 N(D)\, dD = \frac{1}{2} \int_0^{\infty} D^3 N(D)\, dD. \tag{5a}$$

Similarly, a mass-weighted mean diameter D_m can be defined as

$$D_m = \frac{E(D^4)}{E(D^3)}, \tag{5b}$$

where E stands for the expected value. Using (4), $f_D(D)$, the gamma pdf described by (2), can be written in terms of D_0 and μ as

$$f_D(D) = \frac{(3.67 + \mu)^{\mu+1}}{\Gamma(\mu + 1) D_0} \left(\frac{D}{D_0}\right)^{\mu} e^{-[(3.67+\mu)(D/D_0)]}. \tag{6}$$

The above form makes the normalized diameter (D/D_0) as the variable rather than D. Several measurables such as water content (W) and rainfall rate (R) can be expressed in terms of the DSD as

$$W = \frac{\pi}{6} \rho_w n_c E(D^3), \quad \text{and} \tag{7}$$

$$R = \frac{\pi}{6} n_c E[v(D) D^3], \tag{8a}$$

where R is the still-air rainfall rate and $v(D)$ is the terminal velocity of raindrops (Gunn and Kinzer 1949). The conventional unit of rainfall rate is millimeters per hour. Converting to this unit, rainfall rate is expressed as

$$R = 0.6\pi \times 10^{-3} n_c E[v(D) D^3] \quad (\mathrm{mm\ h^{-1}}), \tag{8b}$$

where n_c is in cubic millimeters, $v(D)$ in millimeters per second, and D in millimeters.

In order to compare the pdf of D [or, $f_D(D)$] in the presence of varying water contents, the concept of scaling the DSD has been used by several authors (Sekhon and Srivastava 1971; Willis 1984; Testud et al. 2000). The corresponding form of $N(D)$ can be expressed as

$$N(D) = N_w f(\mu) \left(\frac{D}{D_0}\right)^{\mu} \exp\left[-(3.67 + \mu)\frac{D}{D_0}\right], \tag{9}$$

where N_w is the scaled version of N_0 defined in (3):

$$N_w = \frac{N_0}{f(\mu)} D_0^{\mu}, \quad \text{and} \tag{10a}$$

$$f(\mu) = \frac{6}{(3.67)^4} \cdot \frac{(3.67 + \mu)^{\mu+4}}{\Gamma(\mu + 4)}, \tag{10b}$$

with $f(0) = 1$ and $f(\mu)$ is a unitless function of μ. One interpretation of N_w is that it is the intercept of an equivalent exponential distribution with the same water content and D_0 as the gamma DSD (Bringi and Chandrasekar 2001). Thus N_w, D_0, and μ form the three parameters of the gamma DSD.

3. Raindrop shape and implication for polarimetric radar measurements

The equilibrium shape of raindrops is determined by a balance of hydrostatic, surface tension, and aerodynamic forces. The commonly used model for raindrops assumes oblate spheroidal shapes, with the axis ratio b/a, where b and a are the semiminor and the semimajor axis lengths, respectively. Pruppacher and Beard (1970) give a simple model for the axis ratio (r) based on a linear fit to wind tunnel data as

$$r = 1.03 - 0.062D; \qquad 1 \le D \le 9 \text{ mm}. \tag{11}$$

Rotating linear polarization data in heavy rain (Hendry et al. 1987) has indicated that raindrops fall with the mean orientation of their symmetry axis in the vertical direction. The large swing in the crosspolar power in their data implies a high degree of orientation of drops with the standard deviation of canting angles estimated to be around 6° assuming a Gaussian model. It is reasonable to assume that the standard deviation of canting angles is in the range 5°–10° (Bringi and Chandrasekar 2001).

a. Differential reflectivity

The differential reflectivity can be written as (Seliga and Bringi 1976)

$$10 \log_{10}\frac{E[\sigma_{hh}(D)]}{E[\sigma_{vv}(D)]} = 10 \log_{10}(\xi_{dr}), \quad (12)$$

where the symbol E represents expectation and σ_{hh} and σ_{vv} are the cross sections at horizontal and vertical polarizations, respectively.

Seliga and Bringi (1976) showed that for an exponential distribution and axis ratio given by (11), Z_{dr} can be expressed as a function of the median volume diameter D_0. This microphysical link between a radar measurement and a parameter of the DSD is important. More fundamentally, ξ_{dr}^{-1} may be related to the reflectivity factor–weighted mean of $r^{7/3}$ (Jameson 1985). For a more general gamma form, an approximate power-law fit can be derived assuming $-1 \le \mu \le 5$, $0.5 < D_0 < 2.5$ mm, and N_w chosen to be consistent with thunderstorm rain rates. Using the fit recommended by Andsager et al. (1999) for the Beard and Chuang (1987) equilibrium shapes, power-law fits to D_0 and D_m can be derived as

$$D_0 = 1.619(Z_{dr})^{0.485} \quad \text{(mm)}, \quad (13a)$$

$$D_m = 1.529(Z_{dr})^{0.467} \quad \text{(mm)}, \quad (13b)$$

where Z_{dr} is in decibels and the fits are valid at S-band frequency (near 3 GHz; Bringi and Chandrasekar 2001).

b. Specific differential phase

The relation between specific differential phase (K_{dp}) and the water content and raindrop axis ratio was described by Jameson (1985). Following Bringi and Chandrasekar (2001) a simple approach based on Rayleigh–Gans scattering is described here to derive this relation.

The specific differential phase can be expressed as

$$K_{dp} = \frac{2\pi}{k_0}\mathrm{Re}[E(f_h - f_v)] \quad (\text{deg km}^{-1}), \quad (14)$$

where k_0 is the free space propagation constant, and f_h, f_v are the forward scatter amplitudes at horizontal and vertical polarization, respectively. For Rayleigh–Gans scattering, (14) reduces to

$$K_{dp} = \frac{\pi k_0}{12}\,\mathrm{Re}\left\{E\left[D^3\left(\frac{\epsilon_r - 1}{1 + \frac{1}{2}(1 - \lambda_z)(\epsilon_r - 1)} - \frac{\epsilon_r - 1}{1 + \lambda_z(\epsilon_r - 1)}\right)\right]dD\right\}, \quad (15a)$$

where ϵ_r is the dielectric constant and the depolarizing factor λ_z is given by

$$\lambda_z = \frac{1 + f^2}{f^2}\left(1 - \frac{1}{f}\tan^{-1} f\right), \quad \text{and} \quad (15b)$$

$$f^2 = \frac{1}{r^2} - 1. \quad (15c)$$

The above expectation can be substantially simplified by recognizing that

$$\mathrm{Re}\left[\frac{\epsilon_r - 1}{1 + \frac{1}{2}(1 - \lambda_z)(\epsilon_r - 1)} - \frac{\epsilon_r - 1}{1 + \lambda_z(\epsilon_r - 1)}\right] \cong c(1 - r), \quad (16)$$

where c is approximately constant varying between 3.3 and 4.2 with r from 1 to 0.5. This range of c is valid for ϵ_r of water at microwave frequencies in the range 3–30 GHz. Substituting (16) in (15a) results in

$$K_{dp} = \frac{\pi k_0 c}{12}\int D^3(1 - r)N(D)\,dD \quad (17a)$$

$$= \frac{\pi}{\lambda} \times \frac{c}{\rho_w}\int \frac{\pi}{6}\rho_w D^3(1 - r)N(D)\,dD \quad (17b)$$

$$= \frac{\pi c W}{\lambda \rho_w}\left[1 - \frac{E(rD^3)}{E(D^3)}\right], \quad (17c)$$

where W is the rainwater content, ρ_w is the water density, E stands for expectation over the DSD, and λ is the wavelength. The ratio of expectations in (17c) can be defined as the mass-weighted mean axis ratio $\overline{r_m}$. In terms of conventional units for W in grams per cubic meters, $\rho_w = 1$ g cm^{-3}, and λ in meters, (17c) can be reduced to

$$K_{dp} = \left(\frac{180}{\lambda}\right) \times 10^{-3} c W(1 - \overline{r_m}) \quad (\text{deg km}^{-1}), \quad (18)$$

where $c \cong 3.75$ is both dimensionless and independent of wavelength. This result links the specific differential phase with parameters of the DSD (Jameson 1985). If the equilibrium axis ratio model given in (11) is used in (18) then K_{dp} is given by

$$K_{dp} = \left(\frac{180}{\lambda}\right) \times 10^{-3} c W(0.062) D_m \quad (\text{deg km}^{-1}). \quad (19)$$

Thus, K_{dp} is related to the product of D_m and water content. Though the above result was obtained using the Rayleigh–Gans approximation, it is valid up to 13 GHz (Bringi and Chandrasekar 2001).

c. Mean raindrop shape derived from polarimetric radar measurements

Field studies of Tokay and Beard (1996) indicate that raindrops from 1 to 4 mm oscillate. Andsager et al. (1999) show that oscillations result in an upward shift of the mean axis ratio versus diameter curve, specially in the 1- to 4-mm range. Gorgucci et al. (2000) assumed a simple linear model for axis ratio versus size of the form

$$r = 1 - \beta D \quad (20)$$

and derived radar-based estimators of β. They also showed that β decreases slightly with increasing reflectivity (or, on the average, the axis ratio is smaller than the equilibrium axis ratio) perhaps indicating raindrop oscillations.

It was shown in section 3a that ξ_{dr}^{-1} is related to the reflectivity weighted axis ratio. Similar dependence on K_{dp} can be derived from (18). Let $p(r)$ be the probability density function of the axis ratio for a given diameter. The expression for K_{dp} can be generalized as (Bringi and Chandrasekar 2001)

$$K_{dp} = \frac{2\pi c^*}{k_0} \int D^3 N(D) \int (1 - r) p(r)\, dr\, dD \quad (21)$$

$$= \frac{2\pi c^*}{k_0} \int D^3 N(D)[1 - E(r)]\, dD, \quad (22)$$

where $E(r)$ is the mean value of r, and c^* is a constant. The functional dependence of $E(r)$ versus D may be modeled as in (20). Using the linear model in (20), Gorgucci et al. (2000) showed the variations of Z_{dr} and K_{dp} with respect to β, and in turn derived an estimator for β based on polarimetric radar measurements. This can be used subsequently in algorithms relating Z_{dr} and K_{dp} to the parameters of the DSD, which gives rise to a methodology for estimating the gamma DSD parameters based on radar measurements.

4. Estimators of the gamma DSD parameters

Seliga and Bringi (1976) showed that for an exponential distribution, the two parameters of the DSD, namely N_w and D_0, can be estimated using Z_{dr} and Z_h. They used a two-step procedure where they estimated D_0 using an equilibrium raindrop shape model and subsequently used that in the expression for Z_h to estimate N_w. This procedure can essentially be applied for a gamma DSD, and generalized to account for raindrop oscillations using the linear model in (20). The procedure for estimating the gamma DSD parameters is as follows: first, estimate β using the algorithm described by Gorgucci et al. (2000) and, subsequently, estimate D_0, N_w, and μ, recognizing the right β value.

a. Estimation of D_0

It was noted in section 3a that D_0 can be estimated from Z_{dr} as a simple power-law expression (13a). This parameterization was based on the Beard and Chuang (1987) equilibrium axis ratios and essentially corresponds to a fixed equivalent β. Gorgucci et al. (1994) obtained approximate parameterizations for Z_h and Z_v of the form

$$Z_h = c_h g_h(\mu) N_0 \left(\frac{D_0}{3.67 + \mu}\right)^{\alpha_h}, \quad (23a)$$

$$Z_v = c_v g_v(\mu) N_0 \left(\frac{D_0}{3.67 + \mu}\right)^{\alpha_v}, \quad (23b)$$

where c_h, c_v, $g_h(\mu)$, $g_v(\mu)$, α_h, and α_v are constants that depend on h and v polarizations. From the above and with some modest algebra, it can be shown that a parameterization for D_0 can be pursued of the form

$$\hat{D}_0 = a_1 Z_h^{b_1} (\xi_{dr})^{c_1}, \quad (24)$$

where $\xi_{dr} = 10^{0.1 Z_{dr}}$ is the differential reflectivity in linear scale, and Z_h is the reflectivity factor at horizontal polarization (in mm^6 m^{-3}). Though the above parameterization form was obtained from the approximation in (23), the coefficients in (24) can be derived from the simulation of gamma DSDs directly as follows. Once the gamma DSD is given in the form in (9), it is straightforward to compute radar parameters such as Z_h, Z_{dr}, and K_{dp}. The mean axis ratio versus D relation is modeled by (20). Under these conditions and at a temperature of 20°, Z_h, Z_{dr}, and K_{dp} are computed for widely varying DSD by randomly varying N_w, D_0, and μ over the following ranges:

$$10^3 \le N_w \le 10^5 \quad (\text{mm}^{-1}\ \text{m}^{-3}), \quad (25a)$$

$$0.5 \le D_0 \le 3.5 \quad (\text{mm}), \quad (25b)$$

$$-1 \le \mu \le 5, \quad (25c)$$

with the constraint $R < 300$ mm h^{-1}. While D_0 and μ are varied randomly over their respective ranges, $\log_{10} N_w$ is randomly varied over its range. This range falls within the range of parameters suggested by Ulbrich (1983). Once Z_h, Z_{dr}, and K_{dp} values are simulated, a nonlinear regression analysis is performed to estimate the coefficients a_1, b_1, c_1. Though these coefficients are accurate for a single β, c_1 changes significantly with β. Figure 1 shows the plot of the coefficients a_1, b_1, c_1 as a function of β to demonstrate the sensitivity. This variation of c_1 with β can be further parameterized by fitting power-law expressions. These coefficients are (valid for S band)

$$a_1 = 0.56, \quad (26a)$$

$$b_1 = 0.064, \quad (26b)$$

$$c_1 = 0.024\beta^{-1.42}. \quad (26c)$$

In summary, D_0 can be estimated by first estimating β using the approach of Gorgucci et al. (2000) as

$$\beta = 2.08 Z_h^{-0.365} K_{dp}^{0.380} \xi_{dr}^{0.965} \quad (\text{mm}^{-1}), \quad (27)$$

and then using coefficients (26) in (24). For the equilibrium axis ratios (24) reduces to

$$\hat{D}_0 = 0.56\ Z_h^{0.064} \xi_{dr}^{1.245}\ (\text{mm}), \quad (28a)$$

whereas, when $\beta = 0.0475$ (typical for tropical rain, discussed in section 6),

$$\hat{D}_0 = 0.56\ Z_h^{0.064} \xi_{dr}^{1.817}\ (\text{mm}). \quad (28b)$$

Simulations can also be utilized to evaluate the performance of the estimator of D_0 in (24). Figure 2a shows a scatterplot of $\hat{D}_0$ versus true D_0, for widely varying

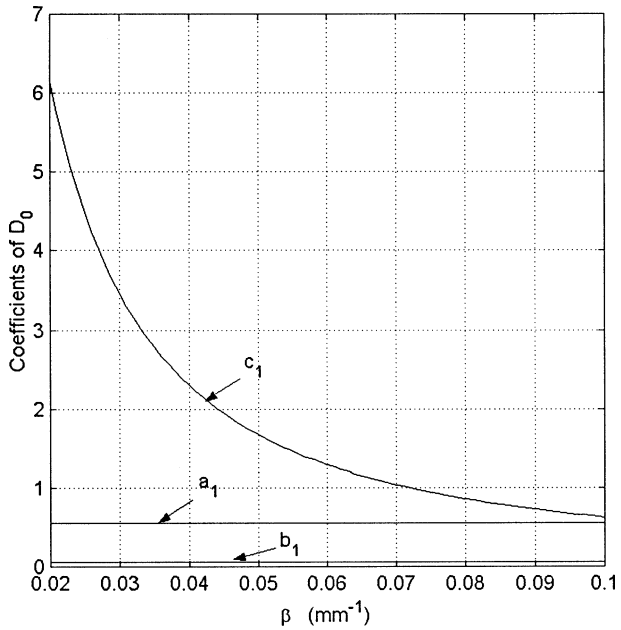

FIG. 1. The coefficients a_1, b_1, c_1 of $D_0(Z_h, Z_{dr})$ algorithm given by (24) as a function of β.

β, and gamma DSD parameters as given by (25). Quantitative analysis of the scatter gives a correlation coefficient of 0.963. It can be seen from Fig. 2a that D_0 is estimated fairly well with negligible bias over a wide range. Figure 2b shows the normalized standard deviation (NSD) of $\hat{D}_0$ as a function of D_0, where NSD is defined as

$$\text{NSD} = \frac{[\text{var}(\hat{D}_0)]^{1/2}}{D_0} = \frac{\text{SD}(\hat{D}_0)}{D_0}, \tag{29}$$

where SD indicates standard deviation. Figure 2b shows that D_0 can be estimated to an accuracy of about 10% when $D_0 > 1$ mm. A similar estimate of D_0 can be derived using K_{dp} and Z_{dr} as

$$\hat{D}_0 = a_2 K_{dp}^{b_2} (\xi_{dr})^{c_2} \text{ (mm)}, \tag{30}$$

where

$$a_2 = 0.41\beta^{-0.34}, \tag{31a}$$

$$b_2 = 0.076, \tag{31b}$$

$$c_2 = 0.097\beta^{-0.97}. \tag{31c}$$

This estimator is similar to the estimator in (24) except that K_{dp} estimates are difficult to obtain at low rain rates. On the other hand, this estimator is immune to variations in absolute calibration of the radar system. Error analysis of the estimator given by (30) yields a correlation coefficient of 0.963. The normalized standard deviation of the estimate of D_0 given (30) is also shown in Fig. 2b. It can be seen that in the absence of any measurement errors these two estimates are comparable. For equilibrium axis ratios this estimator for D_0 reduces to

$$\hat{D}_0 = 1.055\, K_{dp}^{0.076} \xi_{dr}^{1.439} \text{ (mm)}, \tag{32a}$$

whereas, for tropical rain with $\beta \cong 0.0475$ (discussed in section 6),

$$\hat{D}_0 = 1.155\, K_{dp}^{0.076} \xi_{dr}^{1.864} \text{ (mm)}. \tag{32b}$$

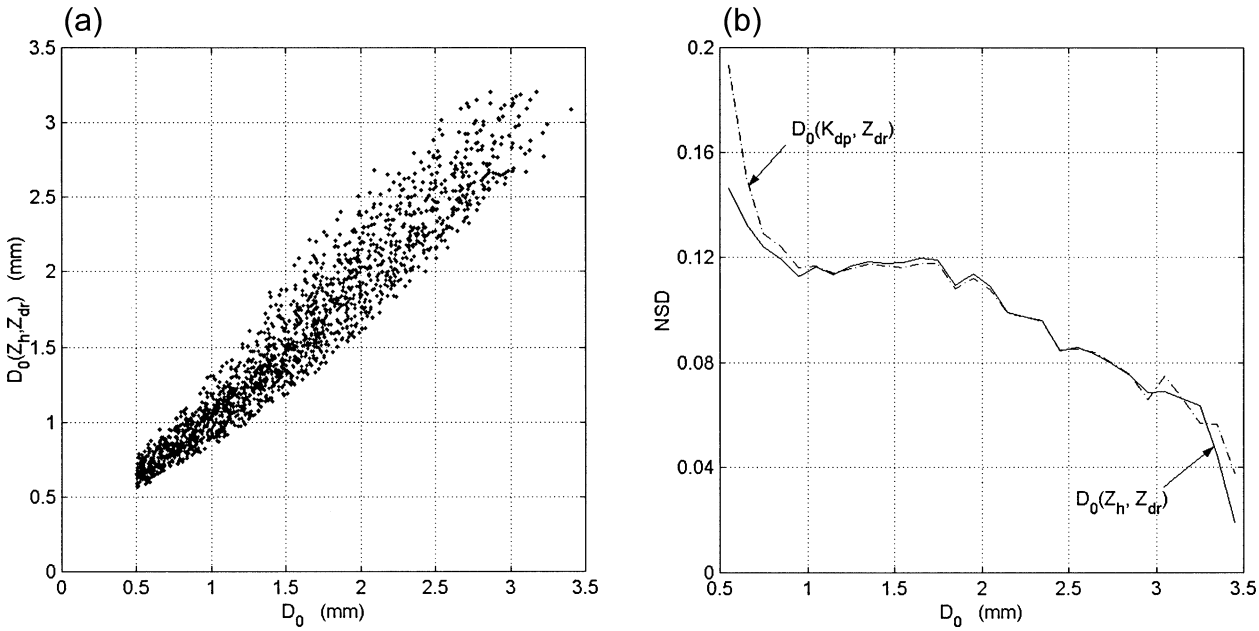

FIG. 2. (a) Scatterplot of $D_0(Z_h, Z_{dr})$ vs the true value of D_0 for widely varying DSD. (b) Normalized standard deviation (NSD) in the estimates of D_0 as a function of the true value of D_0.

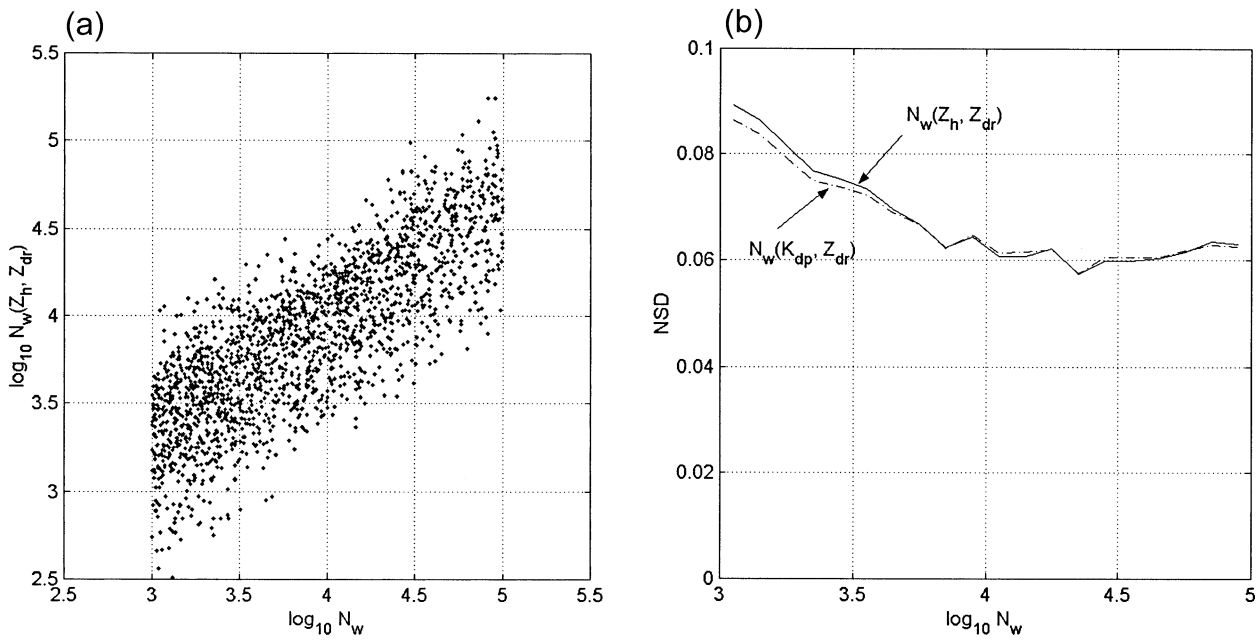

FIG. 3. (a) Scatterplot of $\log_{10}N_w(Z_h, Z_{dr})$ vs the true value of the $\log_{10}N_w$ for widely varying DSD. (b) Normalized standard deviation in the estimates of $\log_{10}N_w$, as a function of $\log_{10}N_w$.

b. Estimation of N_w

Once D_0 is estimated, N_w can be easily estimated using one of the moments of the DSD such as Z_h or K_{dp}. For example, it was shown in (19) that K_{dp} is proportional to the product of W and D_m (or approximately D_0); Z_h can be written in terms of the gamma DSD parameters as (see also Ulbrich and Atlas 1998)

$$\frac{Z_h}{N_w} = F_z(\mu)D_0^7, \tag{33a}$$

where

$$F_z(\mu) = \frac{f(\mu)\Gamma(7+\mu)}{(3.67+\mu)^{7+\mu}}. \tag{33b}$$

For an exponential distribution ($\mu = 0$),

$$N_w = \frac{Z_h}{D_0^7}\frac{(3.67)^7}{6!} = 12.45\frac{Z_h}{D_0^7} \quad (\text{mm}^{-1}\ \text{m}^{-3}). \tag{33c}$$

Thus it can be seen that N_w can be estimated in terms of D_0. However, the estimate of D_0 can be obtained in terms of Z_h and Z_{dr} (or K_{dp} and Z_{dr}). Therefore, a direct estimate of N_w can be pursued of the form

$$\log_{10}(N_w) = a_3 Z_h^{b_3}\xi_{dr}^{c_3}. \tag{34}$$

The variability of a_3, b_3, c_3 can be parameterized in terms of β as

$$a_3 = 3.29, \tag{35a}$$

$$b_3 = 0.058, \tag{35b}$$

$$c_3 = -0.023\beta^{-1.389}. \tag{35c}$$

In summary, the estimator for N_w is obtained as follows. Using Z_h, Z_{dr}, and K_{dp}, first estimate β as given in (27). Subsequently, calculate the coefficients in (35) and use in (34) to estimate N_w. Figure 3a shows a scatterplot of $\log_{10}\hat{N}_w$ versus true $\log_{10}N_w$, where $\log_{10}\hat{N}_w$ is estimated using (34). It can be seen from Fig. 3a that $\log_{10}\hat{N}_w$ is estimated fairly well. Quantitative analysis of the scatter yields a correlation coefficient of 0.831. Figure 3b shows the normalized standard deviation of $\log_{10}N_w$ as a function of $\log_{10}N_w$. It can be seen, from Fig. 3b, that $\log_{10}N_w$ is estimated to a normalized standard deviation of better than 7% when $\log_{10}N_w > 3.5$. Note that due to the wide variability of N_w, $\log_{10}N_w$ is the preferred scale of comparison (similar to dB scale for reflectivity). For equilibrium axis ratios, (34) reduces to

$$\log_{10}\hat{N}_w = 3.29\ Z_h^{0.058}\xi_{dr}^{-1.094}, \tag{36a}$$

whereas for tropical rain with $\beta \cong 0.0475$ (discussed in section 6)

$$\log_{10}N_w = 3.29\ Z_h^{0.058}\xi_{dr}^{-1.585}. \tag{36b}$$

Similarly, another estimate of N_w can be derived using K_{dp} and Z_{dr} as

$$\log_{10}N_w = a_4 K_{dp}^{b_4}(\xi_{dr})^{c_4}. \tag{37}$$

This variability of a_4, b_4, c_4 can be parameterized in terms of β as

$$a_4 = 5.99, \tag{37a}$$

$$b_4 = 0.133\beta^{0.26}, \tag{37b}$$

$$c_4 = -0.042\beta^{-1.16}. \tag{37c}$$

For equilibrium axis ratios, (37) reduces to

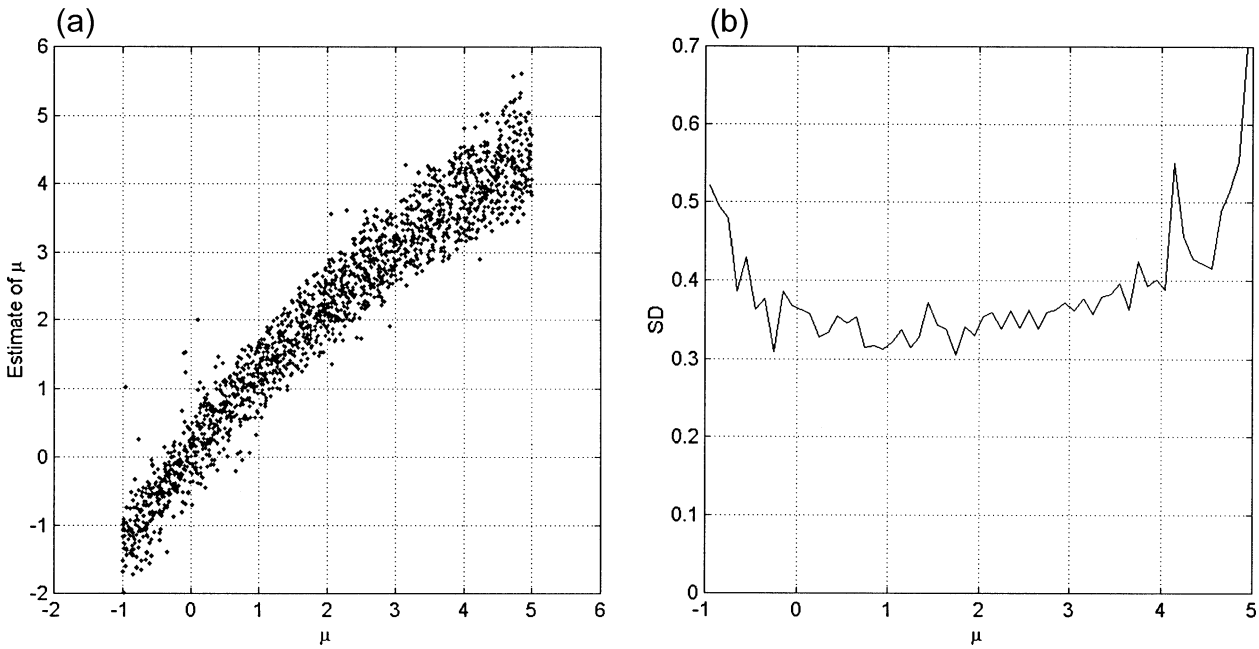

FIG. 4. (a) Scatterplot of the estimates of μ, using Eq. (39) (under the assumption that D_0 is known), vs μ. (b) Standard deviation in the estimates of μ (under the assumption that D_0 is known), as a function of μ.

$$\log_{10}\hat{N}_w = 5.99K_{dp}^{0.065}\xi_{dr}^{-1.057}, \tag{38a}$$

whereas for tropical rain ($\beta \cong 0.0475$)

$$\log_{10}\hat{N}_w = 5.99K_{dp}^{0.06}\xi_{dr}^{-1.44}. \tag{38b}$$

The normalized standard deviation in the estimate of $\log_{10}N_w$ given by (37) is also shown in Fig. 3b. It can be seen from Fig. 3b that the two estimators for $\log_{10}N_w$ are comparable in the absence of the measurement errors.

c. Parameterization of μ

The parameter μ describes the overall shape of the distribution. Once D_0 is estimated, μ can be estimated from the following parameterization, which was constructed empirically as

$$\hat{\mu} = \frac{a_5 D_0^{b_5}}{(\xi_{dr} - 1)} - c_5(\xi_{dr})^{d_5}. \tag{39}$$

The variability of a_5, b_5, c_5, and d_5 can be parameterized in terms of β as

$$a_5 = 200\beta^{1.89}, \tag{40a}$$

$$b_5 = 2.23\beta^{0.039}, \tag{40b}$$

$$c_5 = 3.16\beta^{-0.046}, \tag{40c}$$

$$d_5 = 0.374\beta^{-0.355}; \tag{40d}$$

D_0 calculated from either (24) or (30) can be utilized in (39) to estimate μ. Figure 4a shows the scatterplot of $\hat{\mu}$ given by (39) versus μ under the assumption that D_0 is known. The results of Fig. 4a indicate that μ can be parameterized of the form given by (39) (though it appears complicated). Figure 4b shows the corresponding standard deviation in the estimate of $\hat{\mu}$, which is about 0.3. However, in practice D_0 has to be estimated using (24) or (30), using Z_h, Z_{dr}, and K_{dp}. Estimating μ under such conditions will result in higher error than that projected by Fig. 4b. Estimating μ accurately under practical conditions, especially in the presence of measurement errors is very difficult using the procedures discussed here.

5. Impact of measurement error on the estimates of D_0 and N_w

Estimators of D_0 given by (24) and (30) as well as N_w given by (34) and (37) use measurements of Z_h, Z_{dr}, and K_{dp}. Any error in the measurement of these three parameters will directly translate into errors in the estimates of D_0 and N_w. The three measurements Z_h, Z_{dr}, and K_{dp} have completely different error structures.

The Z_h is based on absolute power measurement and has a typical accuracy of 1 dB. The Z_{dr} is a relative power measurement that can be estimated to an accuracy of about 0.2 dB. The slope of the range profile of the differential propagation phase Φ_{dp} is K_{dp}, which can be estimated to an accuracy of a few degrees. The subsequent estimate of K_{dp} depends on the procedure used to compute the range derivative of Φ_{dp} such as a simple finite-difference scheme or a least squares fit. Using a least squares estimate of the Φ_{dp} profile, the standard deviation of K_{dp} can be expressed as (Gorgucci et al. 1999)

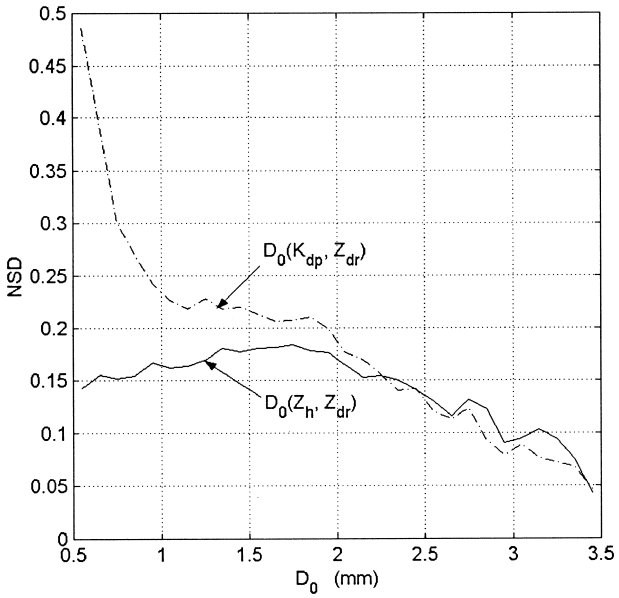

FIG. 5. Normalized standard deviation in the estimates of D_0 as a function of D_0 in the presence of radar measurement errors.

$$\sigma(K_{dp}) = \sqrt{3}\frac{\sigma(\Phi_{dp})}{N\Delta r}\sqrt{\frac{N}{(N-1)(N+1)}}, \quad (41)$$

where Δr is the range resolution of the Φ_{dp} estimate and N is the number of range samples along the path. For a typical 150-m range spacing, and with 2.5° accuracy of Φ_{dp}, K_{dp} can be estimated over a path of 3 km, with a standard error of 0.32° km^{-1}.

The measurement errors of Z_h, Z_{dr}, and K_{dp} are nearly independent. In the following, simulations are used to quantify the error structure of the estimates of D_0 and N_w. The simulation is done as follows. For each gamma DSD the corresponding Z_h, Z_{dr}, and K_{dp} are computed. The random measurement errors are simulated using the procedure described in Chandrasekar et al. (1986). The principal parameters of the simulation are as follows: 1) wavelength $\lambda = 11$ cm; 2) pulse repetition time (PRT) 1 = ms; 3) number of sample pairs used in the estimates is 64; 4) Doppler velocity spectrum width $\sigma_v = 2$ m s^{-1}; 5) copolar correlation between horizontally and vertically polarized signals $\rho_{hv} = 0.99$; 6) range sample spacing is 150 m; and 7) K_{dp} is estimated as a least squares fit over a path consisting of 50 range samples. Subsequently, estimates of D_0 and N_w are obtained using the simulated measurements of Z_h, Z_{dr}, and K_{dp}. There are some practical issues associated with the estimation of D_0 and N_w from radar measurements (or simulated radar measurements). At low rain rates, K_{dp} is small, and in the presence of measurement errors, K_{dp} estimates could be very small (fluctuating around zero). Under this condition (say, when $K_{dp} < 0.2$ deg km^{-1}), (27) cannot be used to estimate β. Therefore, when K_{dp} is small the following procedure is adopted: whenever $K_{dp} < 0.2°$ km^{-1} the equilibrium model for axis ratios are assumed and (28a) and (36a) are used for estimating D_0 and N_w, respectively. It can be noted that (13a) also could be used for estimating D_0, followed by either (33c) or (36b) for N_w. In light rain all these algorithms provide similar results for estimates of N_w and D_0.

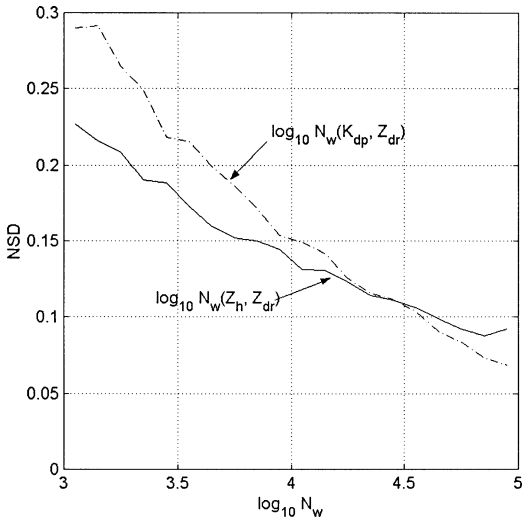

FIG. 6. Normalized standard deviation in the estimates of $\log_{10}N_w$ as a function of $\log_{10}N_w$ in the presence of radar measurement errors.

The normalized standard deviation in the estimates of D_0 and N_w including the effect of measurement error are evaluated and shown in Figs. 5 and 6, respectively. Figure 5 shows the NSD in the estimates of D_0 given by (24) and (30). Comparing Fig. 5 to Fig. 2b it can be seen that in general, there is about a 10% increase in the NSD of D_0 estimate, computed from (24), due to measurement error. The NSD of D_0 estimate from (30) gets worse for smaller D_0 primarily due to the error in K_{dp}. The NSD of the N_w estimates, given by (34) and (37) in the presence of measurement errors, are shown in Fig. 6. Again comparing these to the NSD computations without measurement error (Fig. 3b), a 4% to 16% increase is noted depending on the value of N_w. For an N_w value of 8000 mm^{-1} m^{-3} the NSD of $\log_{10}N_w$ is about 12% in the presence of measurement errors. Once again the estimate of $\log_{10}N_w$ from (37) has higher standard deviation when $N_w < 20\,000$ mm^{-1} m^{-3}. Thus, D_0 and N_w can be estimated fairly well from radar measurements at least for convective rainfall with $R \geq 5$–10 mm h^{-1}. These errors can be further reduced using other techniques such as spatial averaging whenever possible, which may be especially useful for stratiform rain. The following section presents evaluation of the algorithms developed here using disdrometer observations.

6. Evaluation of the algorithms using disdrometer data

The algorithms developed in this paper to estimate D_0 and N_w are applied to data collected with a J–W

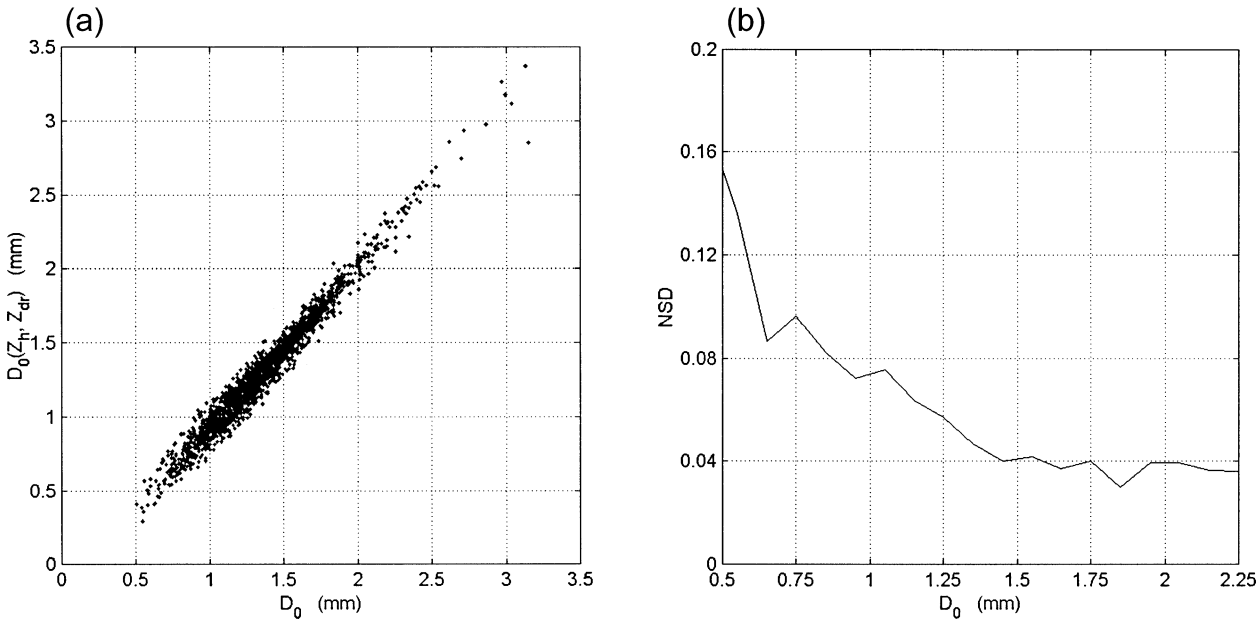

FIG. 7. (a) Scatterplot of the estimate of D_0 computed from simulations of Z_h, Z_{dr}, and K_{dp}, vs the direct estimate of D_0 for DSD obtained from a disdrometer located near Darwin, Australia. There are 2159 two-min DSD samples from the disdrometer. (b) Normalized standard deviation in the estimate of D_0, computed from simulations of Z_h, Z_{dr}, and K_{dp}, vs the direct estimate of D_0 for DSD obtained from a disdrometer located near Darwin, Australia.

impact disdrometer (Joss and Waldvogel 1967) during a rainfall season (covering about 3 months) from Darwin, Australia. This dataset was collected by the Bureau of Meteorology Research Center (BMRC) and includes a variety of rainfall types from a tropical regime with rain rates between 1 and 150 mm h^{-1}. The disdrometer data consists of measurements of $N(D)$ in discrete intervals of ΔD at 30-s intervals, which are subsequently averaged over 2 min. While several methods are available to fit the measured $N(D)$ to a gamma form (e.g., Willis 1984), the method used here is based on Bringi and Chandrasekar (2001). First, D_m is estimated using the definition in (5b), that is, as a ratio of the fourth to third moments of the measured $N(D)$. Next the water content W is estimated from the definition in (7). The parameter N_w in (9) is then calculated as the intercept of the equivalent exponential DSD that has the same W and D_m as the measured $N(D)$, as

$$N_w = \frac{4^4}{\pi\rho_w}\left(\frac{10^3 W}{D_m^4}\right) \quad (\text{mm}^{-1}\ \text{m}^{-3}) \tag{42}$$

(where W is in g cm^{-3}, D_m is in mm, and the water density ρ_w is in g cm^{-3}). Finally, the parameter μ is estimated by minimizing the absolute deviation between observed $\log_{10}N(D)$ and that given by (9). Here, D_0 is estimated from D_m as (Ulbrich 1983)

$$D_0 = D_m \frac{(3.67 + \mu)}{(4 + \mu)}. \tag{43}$$

Once the set of (N_w, D_0, μ) parameters are obtained, the radar observables Z_h, Z_{dr}, and K_{dp} are simulated based on the following assumptions:

1) axis ratio versus D relation based on the fit proposed by Andsager et al. (1999) for D up to 4 mm; beyond 4 mm, the equilibrium axis ratios of Beard and Chuang (1987) are used;
2) Gaussian canting angle distribution with mean of 0° and standard deviation 10°; and
3) truncation of the gamma DSD at $D_{\max} = 3.5\, D_m$ [see Ulbrich and Atlas (1998) for a discussion of the drop truncation of the DSD].

The simulated set of radar observables (Z_h, Z_{dr}, and K_{dp}) when used in (27) gives an ''effective'' β of 0.0475 (for comparison, the equilibrium β is 0.062).

Note that the algorithms for D_0 and N_w are constructed to be insensitive to the actual value of β, so that the details of the assumptions used in simulating the set of radar observables are not of particular relevance, and this fact is indeed the power of the proposed D_0 and N_w algorithms in (24), (30), (34), and (37). In order to evaluate these algorithms using disdrometer measurements, the simulated values of Z_h, Z_{dr}, and K_{dp} are used in (24), (34), and (39) to calculate $\hat{D}_0$, $\hat{N}_w$, and $\hat{\mu}$, which are then compared against D_0, N_w, and μ estimated by gamma fits to the set of measured $N(D)$. Once again, to be consistent when $K_{dp} < 0.2°$ km^{-1}, the estimates are computed using the practical approximation discussed in section 5. Figure 7a shows the D_0 comparisons while Fig. 7b shows the NSD. Note that the $\hat{D}_0$ algorithm can retrieve the ''true'' D_0 quite

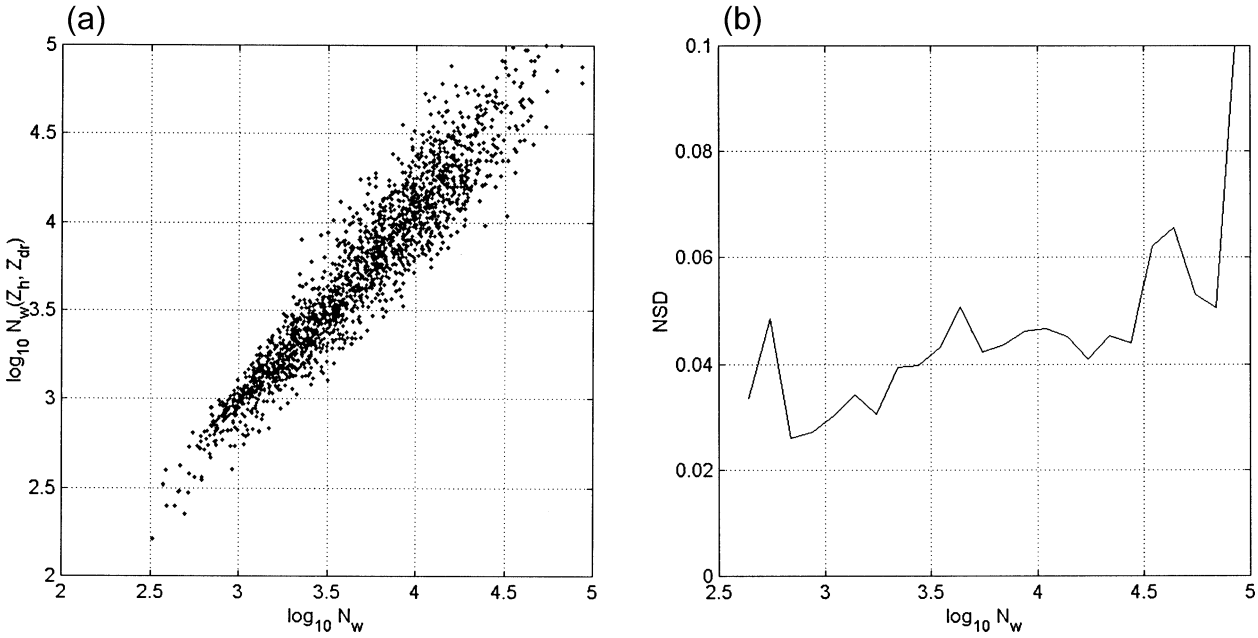

FIG. 8. (a) Scatterplot of $\log_{10}N_w(Z_h, Z_{dr})$, vs the direct estimate of $\log_{10}N_w$ for DSD obtained from a disdrometer located near Darwin, Australia. (b) Normalized standard deviation of $\log_{10}N_w(Z_h, Z_{dr})$, vs the direct estimate of $\log_{10}N_w$ for DSD obtained from a disdrometer located near Darwin, Australia.

accurately (NSD $<$ 7%) especially for $D_0 > 1$ mm. As expected the D_0 estimates get very accurate for higher values. The $\log_{10}(N_w)$ comparison are shown in Fig. 8a, while Fig. 8b shows the NSD. The scatter in Fig. 8a shows that the accuracy in the retrieval of $\log_{10}N_w$ is quite high ($<$5%) for $N_w > 1000$ mm^{-1} m^{-3} (for reference, the Marshall–Palmer value for N_w is 8000 mm^{-1} m^{-3}). Figure 9a shows the μ comparison, while Fig. 9b shows the corresponding standard deviation. The results of Fig. 9 show that it is difficult to retrieve μ with any

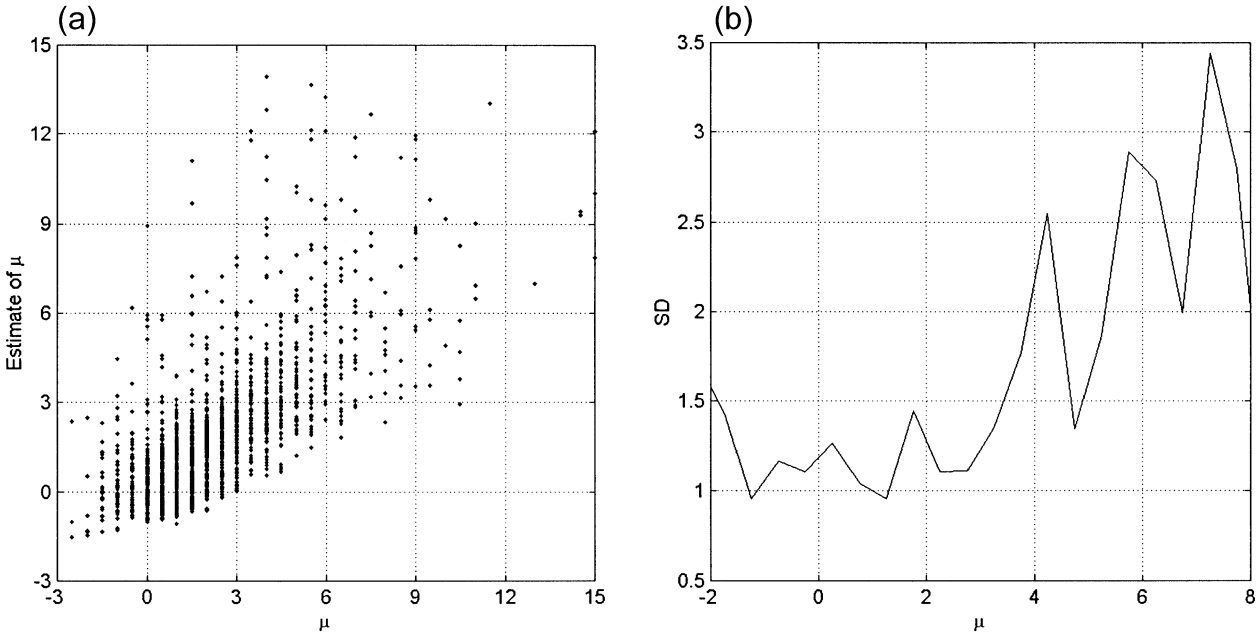

FIG. 9. (a) Scatterplot of the estimates of μ, vs the direct estimate of μ for DSD obtained from a disdrometer located near Darwin, Australia. (b) Standard deviation in the estimates of μ as a function of the direct estimate of μ for DSD obtained from a disdrometer located near Darwin, Australia.

reasonable accuracy with the current algorithms, though it may be possible to distinguish between certain ranges of μ, for example, $\mu = 0$ as opposed to $\mu > 5$, which may be sufficient in practice.

7. Summary and conclusions

One of the long-standing goals of polarimetric radar has been the estimation of the parameters of the raindrop size distribution. Estimators for the parameters of a three-parameter gamma model, namely D_0, N_w, and μ, are developed in this paper based on the radar observations Z_h, Z_{dr}, and K_{dp}. The behavior of the three radar observations Z_h, Z_{dr}, and K_{dp} are influenced by the underlying DSD, and the mean shape of raindrops. Reflectivity Z_{dr} is proportional to the reflectivity-weighted axis ratio, whereas K_{dp} is proportional to the volume-weighted deviation of the axis ratio from unity. In addition, reflectivity is proportional to the sixth moment of the DSD, with corresponding variability due to polarization. Thus, the different polarimetric radar observations weight the DSD differently. It should be noted that the DSD estimates computed here correspond to radar measurements from the radar resolution volume. Among the three measurements (Z_h, Z_{dr}, and K_{dp}), Z_{dr} is the most closely related to a parameter of the DSD, namely D_0. Gorgucci et al. (2000) described a procedure to estimate the mean shape–size relation of raindrops based on a simple linear model. Therefore, after the prevailing shape–size relation is established, Z_{dr} can be used to estimate D_0 directly. This concept is implemented in this paper as an algorithm to estimate D_0 from Z_h, Z_{dr}, and K_{dp}. Statistical analysis of the estimator of D_0 indicates that it can be estimated to an accuracy of 10% when D_0 is 2 mm (and similar accuracies at the other D_0 values). Once D_0 is estimated, other measurements such as Z_h or K_{dp} can be used to estimate N_w, to a normalized standard deviation of about 6.5% when $N_w = 8000\ \text{mm}^{-1}\ \text{m}^{-3}$, and similar order at the other values. The estimation of μ is not easy because of the least influence of this parameter on the three measurements Z_h, Z_{dr}, and K_{dp}. Therefore, the parametric estimates of μ derived are not as accurate. Measurement errors in Z_h, Z_{dr}, and K_{dp} play a key role in the final accuracy of DSD estimates. Reflectivities Z_h and Z_{dr} are based on backscatter power measurement whereas K_{dp} is a forward scatter phase measurement. In addition, Z_{dr} is a differential power measurement between two correlated signals, and can be measured accurately. This high degree of accuracy in Z_{dr} translates to high accuracy in D_0. However, to estimate the prevailing mean shape–size relation, K_{dp} is needed that is relatively noisy at low rainrates. A hybrid approach is implemented in this paper such that when $K_{dp} \leq 0.2$ deg km^{-1} the equilibrium shape model is used to estimate D_0. This procedure yields estimates of D_0 to an accuracy of the order of 15%. Similarly, $\log_{10}N_w$ can be estimated in the presence of measurement error to an accuracy of 15% when $N_w = 8000\ \text{mm}^{-1}\ \text{m}^{-3}$. This accuracy deteriorates to about 20% when N_w is of the order 1000 mm^{-1} m^{-3} but improves to 10% if N_w is of the order 40 000 mm^{-1} m^{-3}. At low rainrates the best estimate of D_0 or N_w is still the original estimates by Seliga and Bringi (1976). At low rainrates accurate estimates of Z_{dr} can be obtained by doing sufficient areal averaging, which can then be used in (13a) to estimate D_0 and a subsequent exponential distribution algorithm given by (33c) to estimate N_w. In the presence of measurement error, μ is difficult to estimate using the procedure described here in a meaningful manner. However, it may be possible to distinguish between $\mu \approx 0$ versus $\mu > 5$, which may be sufficient in practice. The algorithms developed here were applied to one rainy season of disdrometer data collected in Darwin, Australia. The disdrometer analysis indicates that the algorithms work fairly well for the estimation of D_0 and N_w. In summary, the algorithms presented in this paper can be used to estimate the parameters of the raindrop size distribution, from polarimetric radar data at a frequency near 3 GHz (S band).

Acknowledgments. This research was supported partially by the National Group for Defense from Hydrological Hazard (CNR, Italy) and by the Italian Space Agency (ASI). Two of the authors (V. Chandrasekar and V. N. Bringi) acknowledge support from the NASA TRMM program. The disdrometer data were provided by Dr. T. Keenan of the Bureau of Meteorology Research Center. The authors are grateful to P. Iacovelli for assistance rendered during the preparation of the manuscript.

REFERENCES

Andsager, K., K. V. Beard, and N. F. Laird, 1999: Laboratory measurements of axis ratios for large raindrops. *J. Atmos. Sci.,* **56,** 2673–2683.

Aydin, K., H. Direskeneli, and T. A. Seliga, 1987: Dual-polarization radar estimation of rainfall parameters compared with ground-based disdrometer measurements: October 29, 1982, central Illinois experiment. *IEEE Trans. Geosci. Remote Sens.,* **GE-25,** 834–844.

Beard, K. V., and C. Chuang, 1987: A new model for the equilibrium shape of raindrops. *J. Atmos. Sci.,* **44,** 1509–1524.

Bringi, V. N., and V. Chandrasekar, 2001: *Polarimetric Doppler Weather Radar: Principles and Applications.* Cambridge University Press, 636 pp.

——, ——, and R. Xiao, 1998: Raindrop axis ratio and size distributions in Florida rainshafts: An assessment of multiparameter radar algorithms. *IEEE Trans. Geosci. Remote Sens.,* **36,** 703–715.

Chandrasekar, V., V. N. Bringi, and P. J. Brockwell, 1986: Statistical properties of dual polarized radar signals. Preprints, *23d Conf. on Radar Meteorology,* Snowmass, CO, Amer. Meteor. Soc., 154–157.

Gorgucci, E., G. Scarchilli, and V. Chandrasekar, 1999: Specific differential phase shift estimation in the presence of nonuniform rainfall medium along the path. *J. Atmos. Oceanic Technol.,* **16,** 1690–1697.

——, ——, and ——, 2000: Measurement of mean raindrop shape from polarimetric radar observations. *J. Atmos. Sci.,* **57,** 3406–3413.

Gunn, R., and G. D. Kinzer, 1949: The terminal velocity of fall for water droplets in stagnant air. *J. Meteor.*, **6,** 243–248.

Hendry, A., Y. M. M. Antar, and G. C. McCormick, 1987: On the relationship between the degree of preferred orientation in precipitation and dual polarization radar echo characteristics. *Radio Sci.,* **22,** 37–50.

Jameson, A. R., 1985: Microphysical interpretation of multiparameter radar measurements in rain. Part III: Interpretation and measurement of propagation differential phase shift between orthogonal linear polarizations. *J. Atmos. Sci.,* **42,** 607–614.

Joss, J., and A. Waldvogel, 1967: A raindrop spectrograph with automatic analysis. *Pure Appl. Geophys.*, **68,** 240–246.

Pruppacher, H. R., and K. V. Beard, 1970: A wind tunnel investigation of the internal circulation and shape of water drops falling at terminal velocity in air. *Quart. J. Roy. Meteor. Soc.*, **96,** 247–256.

Sachidananda, M., and D. S. Zrnić, 1987: Rain rate estimates from differential polarization measurements. *J. Atmos. Oceanic Technol.,* **4,** 588–598.

Sekhon, R. S., and R. C. Srivastava, 1971: Doppler radar observations of drop-size distributions in a thunderstorm. *J. Atmos. Sci.*, **28,** 983–994.

Seliga, T. A., and V. N. Bringi, 1976: Potential use of the radar reflectivity at orthogonal polarizations for measuring precipitation. *J. Appl. Meteor.*, **15,** 69–76.

——, and ——, 1978: Differential reflectivity and differential phase shift: Applications in radar meteorology. *Radio Sci.,* **13,** 271–275.

Testud, J., E. L. Bouar, E. Obligis, and M. Ali-Mehenni, 2000: The rain profiling algorithm applied to polarimetric weather radar. *J. Atmos. Oceanic Technol.,* **17,** 332–356.

Tokay, A., and K. V. Beard, 1996: A field study of raindrop oscillations. Part I: Observations of size spectra and evaluation of oscillation causes. *J. Appl. Meteor.,* **35,** 1671–1687.

Ulbrich, C. W., 1983: Natural variations in the analytical form of raindrop size distributions. *J. Climate Appl. Meteor.,* **22,** 1764–1775.

——, and D. Atlas, 1998: Rainfall microphysics and radar properties: Analysis methods for drop size spectra. *J. Appl. Meteor.,* **37,** 912–923.

Willis, P. T., 1984: Functional fits to some observed drop size distribution and parameterization of rain. *J. Atmos. Sci.,* **41,** 1648–1661.